Journal of Cerebral Blood Flow & Metabolism (2010) 30, 1914–1927

www.jcbfm.com

JCBFM Open

Limitations of collateral flow after occlusion of a single cortical penetrating arteriole

Nozomi Nishimura[1,3], Nathanael L Rosidi[1,3], Costantino Iadecola[2] and Chris B Schaffer[1]

[1]*Department of Biomedical Engineering, Cornell University, Ithaca, New York, USA;* [2]*Department of Neurology and Neuroscience, Weill Cornell Medical College, New York, New York, USA*

Occlusions of penetrating arterioles, which plunge into cortex and feed capillary beds, cause severe decreases in blood flow and are potential causes of ischemic microlesions. However, surrounding arterioles and capillary beds remain flowing and might provide collateral flow around the occlusion. We used femtosecond laser ablation to trigger clotting in single penetrating arterioles in rat cortex and two-photon microscopy to measure changes in microvessel diameter and red blood cell speed after the clot. We found that after occlusion of a single penetrating arteriole, nearby penetrating and surface arterioles did not dilate, suggesting that alternate blood flow routes are not actively recruited. In contrast, capillaries showed two types of reactions. Capillaries directly downstream from the occluded arteriole dilated after the clot, but other capillaries in the same vicinity did not dilate. This heterogeneity in capillary response suggests that signals for vasodilation are vascular rather than parenchymal in origin. Although both neighboring arterioles and capillaries dilated in response to topically applied acetylcholine after the occlusion, the flow in the territory of the occluded arteriole did not improve. Collateral flow from neighboring penetrating arterioles is neither actively recruited nor effective in improving blood flow after the occlusion of a single penetrating arteriole.
Journal of Cerebral Blood Flow & Metabolism (2010) **30,** 1914–1927; doi:10.1038/jcbfm.2010.157; published online 15 September 2010

Keywords: collateral flow; imaging; stroke; two-photon microscopy; vasodilation; vasoregulation

Introduction

In the healthy brain, the cerebral vasculature is highly regulated and demonstrates an impressive capacity to control the distribution of blood flow with spatial and temporal precision. For example, the brain vasculature can reroute flow toward specific groups of active neurons as small as a single cortical column (Attwell and Iadecola, 2002). This neurovascular coupling has important scientific and clinical implications because it provides the basis for localizing normal and abnormal brain function using methods such as functional magnetic resonance imaging (Ogawa *et al*, 1990). The neocortex in both rodents and humans has an interconnected network of surface arterioles that consists of many loops (Blinder *et al*, 2010; Schaffer *et al*, 2006; Vander Eecken and Adams, 1953). To feed the capillaries within the cortex, penetrating arterioles branch off surface arterioles and plunge perpendicularly into the brain. It has been suggested that this combination of a highly redundant network of surface arterioles and nonredundant penetrating arterioles might serve to facilitate rerouting of flow from one region to another (Nishimura *et al*, 2007). Such a network might provide a mechanism for flow redistribution not only during normal neurovascular coupling but also in response to vascular occlusions. In experimental models of occlusion of large cerebral arteries, such as the middle cerebral artery (MCA), acute (Belayev *et al*, 2002; Shih *et al*, 2009; Tomita *et al*, 2005; Wei *et al*, 1998) and chronic (Coyle and Heistad, 1987) dilation of cortical arteries and arterioles has been observed, suggesting that a mechanism for compensatory collateral flow is activated. However, it is not known whether such compensatory routing mechanisms are activated after occlusions of smaller vessels such as penetrating arterioles.

Cortical microinfarcts, 400 to 500 μm in size, presumably resulting from occlusion of single cortical arterioles, have been recognized as a prevalent cause of focal neurologic deficits as well as cognitive impairment (Kovari *et al*, 2004; Vermeer *et al*, 2003). However, the hemodynamic mechanisms underlying such lesions are poorly understood. Recent developments in optical

Correspondence: Professor CB Schaffer, Department of Biomedical Engineering, Cornell University, B57 Weill Hall, Ithaca, NY 14853, USA.
E-mail: cs385@cornell.edu
[3]These authors contributed equally to this work.
NN received a postdoctoral grant from the American Heart Association (09POST2250177) and a L'Oréal USA Fellowship for Women in Science; CI received funding from the National Institute of Health (NS37853); and CBS received funding from the American Heart Association (0735644T) and the Ellison Medical Foundation (AG-NS-0330-06).
Received 8 March 2010; revised 30 June 2010; accepted 12 August 2010; published online 15 September 2010

techniques enable the occlusion of only a single segment of an arteriole or capillary (Nishimura *et al*, 2006, 2007; Schaffer *et al*, 2006). These methods, in combination with two-photon excited fluorescence (2PEF) microscopy, provide the tools to study the changes in blood flow and role of active vascular regulation after an occlusion at the level of single microvessels. Experiments with clots in surface arterioles established that there is great redundancy in the surface arteriole network, which provides alternate routes for blood flow around the occluded vessel (Schaffer *et al*, 2006). In contrast, occlusions in penetrating arterioles, which have little redundancy, result in severe decreases in capillary blood flow in a region $\sim 500\,\mu$m in diameter (Nishimura *et al*, 2007), indicating that existing collateral flow is limited. However, it is not known whether the capacity for compensatory flow has been maximized or if additional compensation by vessel dilation might be possible.

In this study, we sought to determine whether the vasculature surrounding an occluded penetrating arteriole is recruited to provide collateral flow to alleviate blood flow decreases. First, we examined whether occlusion of a penetrating arteriole causes active vasodilation in the neighboring penetrating and surface arterioles similar to the dilation observed after occlusion of larger cerebral vessels. Surprisingly, we found no such response. We then examined the effect of the occlusion on the diameter and flow in capillaries around the occluded vessel and found that the only capillaries to dilate were those directly downstream from the occluded vessel; these capillaries also slowed drastically as a result of the clot. Finally, we examined whether the capillary blood flow in the territory of the occluded arteriole could be improved by forcing the neighboring arterioles to dilate, but found that although applying a vasodilator leads to overall increases in flow, it does not resolve the severe blood flow decreases in capillaries downstream from the clot.

Materials and methods

Surgical Preparation

All animal procedures were approved by Cornell University Institutional Animal Care and Use Committee. Fifty-nine male Sprague-Dawley rats (Harlan, Inc, South Easton, MA, USA), ranging from 200 to 400 g in weight were used in the experiments. Glycopyrrolate ($50\,\mu$g/100 g rat) was injected intramuscularly to facilitate respiration. Rats were anesthetized by 5% isoflurane and maintained at 1.5% to 2%. Body temperature was kept constant at 37.5°C, with a heating blanket controlled by rectal thermometer (50 to 7053P; Harvard Apparatus, Holliston, PA, USA). A pulse oximeter (MouseOx; Starr Life Sciences Corp., Oakmont, PA, USA) clipped to the hind paw of the rat was used to monitor blood oxygen saturation and heart rate. A local anesthetic, bupivacaine (0.1 mL, 0.125%), was administered at each incision site. The femoral artery was cannulated to monitor blood pressure (BP-1; World Precision Instruments, Sarasota, FL, USA). A tracheotomy was performed to allow intubation for artificial ventilation (SAR-830/P; CWE Inc, Ardmore, PA, USA) and to monitor exhaled carbon dioxide levels (Capstar-100; CWE Inc). Ventilation rates and breath volumes were adjusted to maintain stable end-tidal carbon dioxide. Rats were ventilated with a mix of medical air and the minimum amount of oxygen needed to maintain a minimum arterial blood oxygen saturation of $\sim$95%. Physiological parameters were recorded throughout the experiments to ensure that physiological variables stayed the same during the multiple stages of each imaging session (Supplementary Table S1). Rats were also given 5% (wt/vol) glucose in physiological saline (0.1 mL/100 g rat) subcutaneously every hour to maintain hydration. An $\sim 3 \times 6$-mm^2 craniotomy was performed over the parietal cortex and the dura was removed. Tubing (inner diameter: 0.25 mm, outer diameter: 0.76 mm; Microbore, Tygon, Shanghai, China) was glued at the edge of the craniotomy to allow perfusion of artificial cerebrospinal fluid (ACSF) (Kleinfeld and Delaney, 1996) and acetylcholine (ACh). An 8-mm, No. 1.5 glass cover slip (50201; World Precision Instruments) was then glued over the exposed brain using cyanoacrylate and dental cement (Lang Dental Mfg Co, Wheeling, IL, USA and Co-Oral-Ite Dental Mfg Co., Diamond Springs, CA, USA). The lateral edge of the craniotomy was left without glue, but covered in 1.5% agarose (A9793; Sigma, St Louis, MO, USA) in ACSF to allow for drainage of ACSF and the ACh solution while preventing exposure of the cortex to outside air. In most experiments ($n = 47$), rats were gradually transitioned off of isoflurane and onto urethane (1.5 g/kg (U2500; Sigma)) administered by intraperitoneal injection. Imaging was started 30 minutes after urethane administration. In some experiments ($n = 12$), rats were kept on isoflurane for the entire duration of the experiment. The vasculature was visualized by intravenously injecting 0.3 mL of 5% (wt/vol) solution of 2-MDa fluorescein-conjugated dextran (FD2000S; Sigma) in physiological saline.

Two-Photon Excited Fluorescence Microscopy of Cerebral Vasculature

In vivo vascular measurements were made with a custom-built 2PEF microscope using 800-nm, 87-MHz, 100-femtosecond pulses from a Ti:sapphire laser oscillator (MIRA HP; Coherent, Santa Clara, CA, USA), pumped by a continuous wave laser (Verdi-V18; Coherent, Santa Clara, CA, USA). Laser pulses were prechirped to compensate for dispersion in the microscope with a prism-based compressor (Muller *et al*, 1998). Laser scanning and data acquisition was controlled by MPScope software (Nguyen *et al*, 2006). Images spanning the entire cranial window were taken using a 0.28 numerical aperture $\times 4$ air objective (Olympus, Center Valley, PA, USA). For high-resolution imaging, red blood cell (RBC) speed measurements, vessel diameter measurements, and vascular lesioning, we used a 0.95-numerical aperture, $\times 20$, water immersion objective (Olympus).

To map and categorize the arterioles, capillaries, and venules in the area around the target vessel, stacks of images spaced 1 μm axially were obtained (Supplementary

Text). To measure vessel diameter, we recorded images of individual vessels stepping from above to below the vessel, accumulating at least 20 image frames (~6 seconds). For surface and penetrating arterioles, these frames were axially projected, guaranteeing a measurement across the thickest (middle) portion of the vessel. Diameters were calculated by manual selection of a region of interest that included the vessel segment to be measured. The area above threshold (20% of maximum intensity in the projection) was divided by the length of the measured area to yield an average measure of diameter across a 10 to 50-μm segment. For capillaries, because the motion of the brain made averaging frames impractical, diameters were measured from ~5 to 10 individual frames in which the motion appeared to be minimal and then averaged.

To quantify centerline RBC velocity in individual vessels, linescan measurements were obtained by scanning single vessels at a line rate of 1.7 kHz for 40 seconds and extracting the average speed over this period (Kleinfeld *et al*, 1998; Schaffer *et al*, 2006). In these measurements, the scan is aligned along the vessel axis, which produces diagonal dark streaks in the resulting space-time image due to moving RBCs (which exclude the intravenously injected dye), with the slope of the streaks inversely proportional to the RBC velocity. Slope is calculated with an automated image-processing algorithm (Kleinfeld *et al*, 1998; Schaffer *et al*, 2006). In arterioles, RBC flow (volume of RBCs/time) was taken to be proportional to the product of the centerline RBC velocity and the cross-sectional vessel area, so we calculated the ratio of flow in a vessel before and after an occlusion as

$$\frac{\mathrm{Flow}_{\mathrm{RBC,post}}}{\mathrm{Flow}_{\mathrm{RBC,pre}}} = \frac{R_{\mathrm{post}}^2 v_{\mathrm{post}}}{R_{\mathrm{pre}}^2 v_{\mathrm{pre}}}$$

where v is the centerline RBC speed and R is the vessel radius. The proportionality constant depends on the exact shape of the dependence of RBC speed and hematocrit on radial position in the vessel. We assume this proportionality constant does not change between baseline and later measurements in the same vessel, and thus cancels out in the ratios reported here (Supplementary Text). In penetrating arterioles, RBC velocity and vessel diameter were measured in the portion of the vessel that ran parallel to the cortical surface proximal to where the arteriole dove into the brain. In capillaries, RBCs must travel nearly single file so we report RBC speed and RBC flux (number of RBCs/time) (Supplementary Text). Images and linescans were taken in the same vessels about 1 hour before and after penetrating arteriole occlusion. Approximately 10 to 25 vessels were measured in each animal. Following postocclusion measurements, ACh (A9101; Sigma; 10 μmol/L in ACSF) (Park *et al*, 2008) was topically applied to the neocortex in some animals. Vessels were remeasured starting 10 minutes after topical application of ACh.

Penetrating Arteriole Occlusion by Femtosecond Laser Ablation

Occlusions of penetrating arterioles were produced by damaging the endothelium of targeted vessels using tightly focused femtosecond laser pulses, leading to localized clotting of the vessel (Nishimura *et al*, 2006). Vessels were irradiated with 50 femtosecond, ~0.1 to 2-μJ pulses from a 1-kHz pulse train produced by a Ti:sapphire regenerative amplifier (Legend 1k USP; Coherent) pumped by a Q-switched laser (Evolution 15; Coherent) and seeded by a Ti:sapphire oscillator (Chinhook Ti:sapphire laser; Kapteyn-Murnane Laboratories Inc, Boulder, CO, USA; pumped by Verdi-V6; Coherent, Inc) (Nishimura *et al*, 2006). The imaging and ablation beams were combined using a polarizing beam splitter located just after the scan mirrors of the 2PEF microscope and were focused in the same plane. The energy was varied with neutral density filters and the number of pulses deposited on the targeted vessel was controlled by a mechanical shutter with 2 milliseconds minimum opening time (VMM-D4; Uniblitz, Rochester, NY, USA). During imaging with 2PEF microscopy, the amplified beam was focused in the lumen of the targeted penetrating arteriole in the segment below the surface but proximal to the first capillary branch off the arteriole. To minimize possible collateral damage, we began irradiation with one pulse using an energy that is below the expected damage threshold (~100 nJ at about 100-μm depth). Next, the number of pulses was increased by factors of 10 up to 1,000 pulses with the same energy, often trying each pulse number a few times while watching for signs of vessel damage. The pulse energy was gradually increased by ~25%, and the sequence of increasing pulse number was repeated until some extravasation of fluorescently labeled blood plasma outside the vessel lumen was observed. Once extravasation occurred, multiple nearby areas along the inner wall of the arteriole segment were irradiated with this laser energy and pulse number. Irradiation was continued until RBC motion as visualized in the segment of the penetrating arteriole at the surface of the cortex was stalled. If the occlusion recanalized, irradiation was repeated until the target vessel stopped flowing. Only one occlusion was produced per animal. As an alternative method for producing occlusions, we use photothrombotic clotting (4/59 rats) (Supplementary Text) (Nishimura *et al*, 2007; Schaffer *et al*, 2006; Sigler *et al*, 2008; Watson *et al*, 1985).

Statistical Analysis

Distributions were nonnormal, so nonparameteric statistical tests were necessary. To compare the effects of different anesthetics and other parameters such as occlusion method or vessel type (Figures 1F–1H, 2A–2C, 2G–2I) two-way analysis of variance (ANOVA) on ranks was used (JMP Statistical Software, SAS Institute Inc, Cary, NC, USA). When this yielded significant differences (Figure 1F) or when multiple comparisons analysis was not necessary (Figures 4A and 4B), we compared pairs of groups with the Wilcoxon–Mann–Whitney ranks sum test. Whenever measurements were made in two instances in the same vessels, the more powerful Wilcoxon rank sign test for paired data was used (Figures 6A and 6C). The significance of trends dependent on topological separation from the targeted arteriole was tested with Cuzick's trend test (Cuzick, 1985)

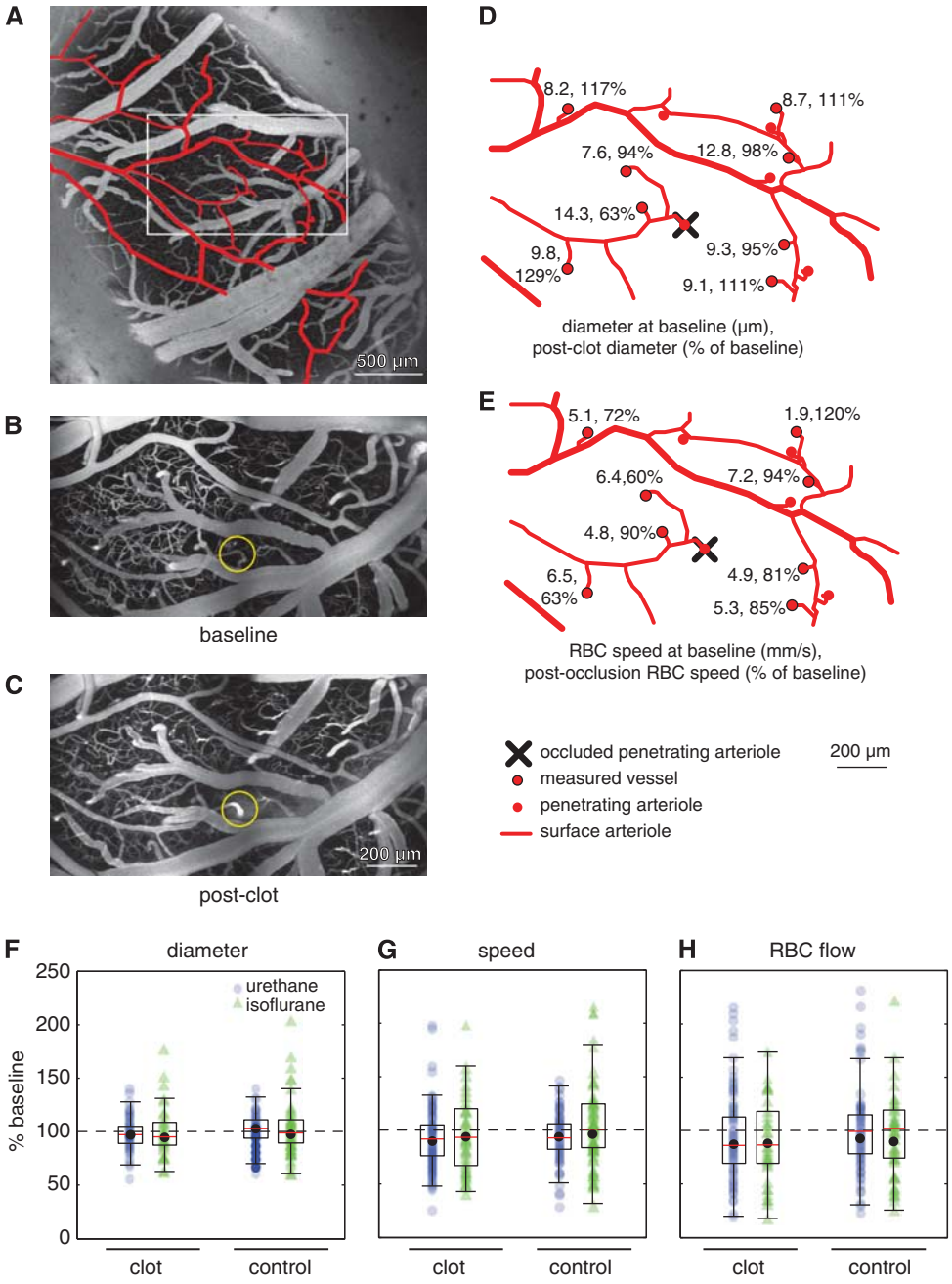

Figure 1 Diameter and flow changes in neighboring penetrating arterioles after the occlusion of a single penetrating arteriole. (**A**) Average projection of a low-magnification two-photon excited fluorescence (2PEF) image stack of rat cortical surface vasculature with arterioles traced in red. Montages (Panavue Image Assembler) of average projections of 2PEF image stacks through 250 μm of cortical vasculature before (**B**) and after (**C**) clotting of a single penetrating arteriole by femtosecond laser irradiation (yellow circle). Images were median filtered. (**D**) Baseline vessel lumen diameter and diameter after penetrating arteriole clot as a percentage of the baseline diameter. (**E**) Baseline average centerline red blood cell speed and speed after penetrating arteriole clot as a percentage of baseline speed. Location of (**B**–**E**) is marked by box in (**A**). Aggregate diameter (**F**), centerline RBC speed (**G**), and RBC flow (**H**) in neighboring penetrating arterioles after occlusion of a single penetrating arteriole (or equivalent time delay only in controls), expressed as a percentage of the baseline value. Each point represents a measurement in a single neighboring penetrating arteriole. In (**F**), the diameter is significantly smaller in the clot experiments as compared with the control experiments under urethane anesthesia (Wilcoxon–Mann–Whitney ranks sum test after two-way analysis of variance on ranks, $P = 0.012$), although the magnitude of this difference is small. Some data points were off the scale of the plot: (**G**) 427% in urethane control experiments, 267%, 369%, 289%, 292% in isoflurane control experiments, (**H**) 296% and 353% in isoflurane clot experiments and 1,114%, 260%, 556%, 540%, 475%, 817%, 568%, 371% in isoflurane control experiments.

(Stats Direct, Altrincham, Cheshire, UK), which is a variant of the Wilcoxon tests (Figures 2A–2C, 4A, 4B, 6B, and 6C). A P value of <0.05 was considered statistically significant for all tests. Matlab was used to generate box plots and trend lines as a function of spatial distance (details in Supplementary Text). We used G*Power (Faul *et al*, 2007)

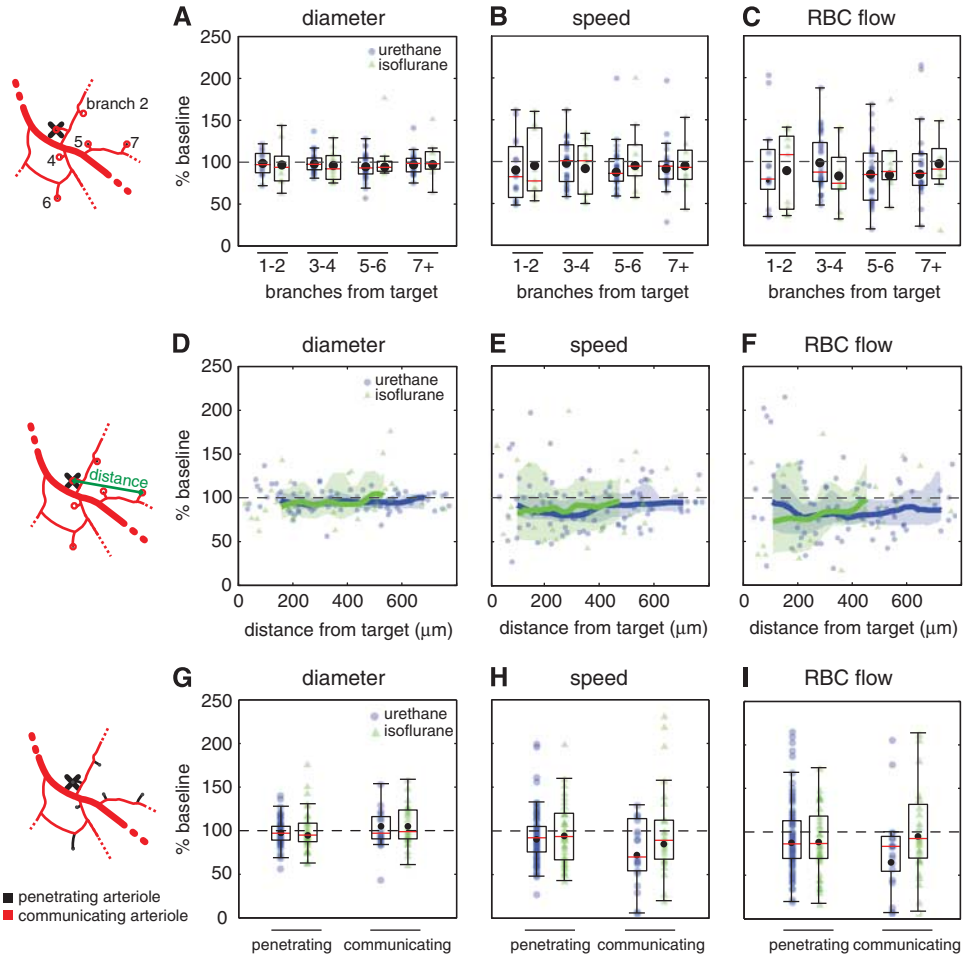

Figure 2 Topology and distance dependence of diameter and flow changes in the neighboring penetrating arterioles after single penetrating arteriole occlusion. Diameter (**A**), centerline red blood cell (RBC) speed (**B**), and RBC flow (**C**) in neighboring penetrating arterioles after a single penetrating arteriole clot, expressed as a percentage of the baseline value, as a function of the number of vessel branches separating the measured and occluded vessels. No significant differences ($P > 0.70$) were detected by two-way analysis of variance on ranks in **A**–**C**. Dependence of postclot diameter (**D**), RBC speed (**E**), and RBC flow (**F**) in neighboring penetrating arterioles, expressed as a percentage of the baseline value, on the distance to the occluded vessel. Solid lines show a running median with 95% confidence intervals indicated by shaded areas. Each point represents a single vessel measurement. Comparison of penetrating and communicating arteriole diameter (**G**), RBC speed (**H**), and RBC flow (**I**) after penetrating arteriole occlusion. Outliers not shown in (**H**) are 264% and 292% for the communicating arteriole, urethane velocity measurements; (**I**) 296% and 353% penetrating arteriole, isoflurane RBC flow, 627% communicating arteriole, urethane RBC flow, and 347% and 442% communicating arteriole, isoflurane RBC flow.

for *post hoc* power analysis using the Wilcoxon–Mann–Whitney test to compare two groups and the Wilcoxon signed-rank test in cases where we had matched pairs (Supplementary Text). Sensitivity was also calculated with G*Power. In all cases, we used $\alpha = 0.05$. A summary of all raw data is given in the Supplementary Information.

Results

The RBC speed and vessel diameter changes caused by penetrating arteriole occlusions were measured in neighboring penetrating and surface arterioles as well as in nearby capillaries in anesthetized, adult, male, Sprague-Dawley rats. We used 2PEF microscopy to image cortical vasculature labeled with intravenously injected fluorescein dextran through closed cortical windows (Figure 1A). Occlusions were produced by focusing femtosecond-duration laser pulses (0.1 to 2-μJ energy) onto the descending segment of a penetrating arteriole just above the first downstream branch (Figures 1B and 1C). Nonlinear absorption of laser energy injures the vessel wall and triggers clotting (Nishimura *et al*, 2006). Before and after occlusion of a single penetrating arteriole, lumen diameter, and RBC speed were measured with 2PEF microscopy in neighboring arterioles (Figures 1D and 1E) and capillaries (Figure 3). The targeted and neighboring penetrating arterioles had similar sizes and speeds (Supplementary Figure S1). Separate animals in which no occlusions were induced with only a matched time delay between vessel measurements were used as controls. We found that the active dilatory responses of neighboring arterioles and nearby

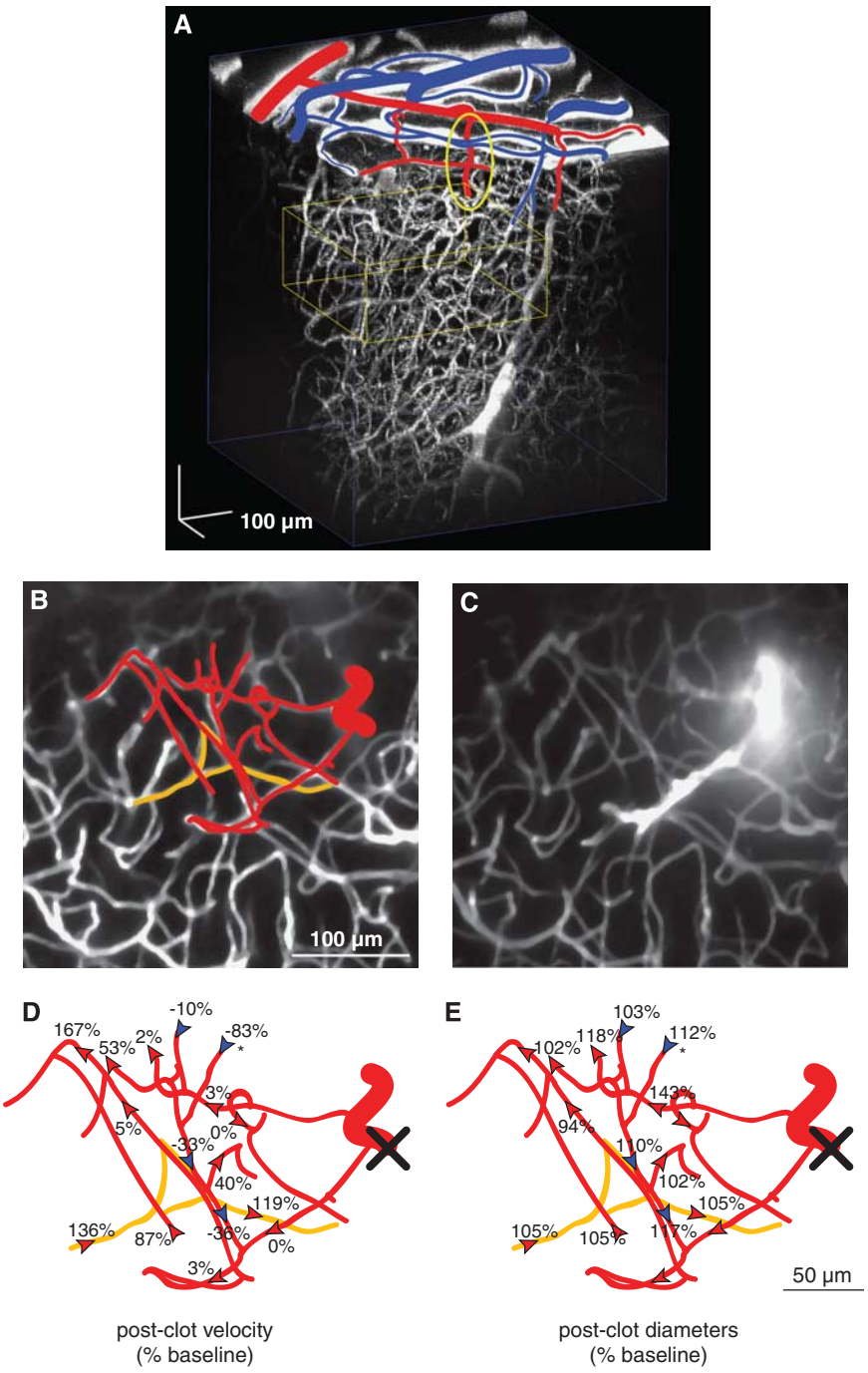

Figure 3 Flow and diameter changes in capillaries after penetrating arteriole occlusion. (**A**) Rendering of two-photon excited fluorescence microscopy image stack of fluorescently labeled vasculature using Voxx (Clendenon *et al*, 2002). A rotating movie of this image stack is shown in the Supplementary Movie. Surface arterioles are marked in red and the venules are marked in blue. Yellow oval indicates the target penetrating arteriole. (**B**) Average projection of image stack before the occlusion through volume marked with yellow box in (**A**), with a subset of capillaries traced. Red vessels were connected to the targeted penetrating arteriole in $\leqslant 10$ branches. Orange vessels did not have any observable connections to the target arteriole. (**C**) Projection of same volume after occlusion of the penetrating arteriole (yellow oval in **A**). Extravasation of fluorescently labeled blood plasma is visible around the occluded arteriole and also along capillaries branching off of the clotted vessel. (**D**) Red blood cell velocity, expressed as a percentage of the baseline value, after occlusion of the penetrating arteriole marked with an X. Arrowheads indicate direction of flow with blue arrows and negative numbers, indicating a reversal in direction after the occlusion. Vessel indicated with an asterisk was five branches away from an unoccluded neighboring penetrating arteriole. (**E**) Postclot vessel diameter expressed as a percentage of the baseline value. Average projections (**B**, **C**) were median filtered.

capillaries after occlusion of a single penetrating arteriole were strikingly different.

Occlusion of a Single Penetrating Arteriole Does Not Initiate Dilation in Neighboring Arterioles

We found no evidence for active vasodilation in neighboring arterioles in response to a penetrating arteriole occlusion (Figures 1D and 1F). As vasoactivity can be altered by anesthesia, we performed the measurements using either urethane (19 occlusions and 12 controls) or isoflurane (7 occlusions and 3 controls) anesthesia during vessel measurements and clot formation (Figures 1F–1H). Rather than dilating, neighboring penetrating arterioles constricted slightly after occlusion (Figure 1F; two-way ANOVA on ranks, $P=0.041$). *Post hoc* sensitivity analysis showed that we should have been able to resolve a 5% increase in diameter under urethane and a 12% increase under isoflurane with a statistical power of 0.8 (Supplementary Text), suggesting that any vasodilation after a penetrating arteriole occlusion is less than these values. We observed a slight, but not statistically significant, drop in both RBC speed and in RBC flow in neighboring penetrating arterioles after the occlusion, indicating that blood flow to the area surrounding the occlusion was mildly decreased (Figure 1G and 1H; two-way ANOVA on ranks $P=0.26$ and $P=0.16$).

To rule out the possibility that nearby or closely connected penetrating arterioles responded differently than distant arterioles, we categorized neighboring penetrating arterioles by the topological separation (i.e., number of vessel branches) and spatial distance from the occluded arteriole. We found no dependence of changes in vessel diameter, RBC speed or RBC flow on topological separation (Figures 2A–2C; Cuzick's trend test, $P>0.14$), indicating that vessels closely or distantly connected to the occluded arteriole are equally unaffected by the occlusion. Similarly, changes in vessel diameter, RBC speed or RBC flow did not depend on the spatial distance between the vessel and the occluded arteriole (Figures 2D–2F). In addition to no dilation in the penetrating arterioles that dive into the brain tissue to feed capillaries, we found that communicating arterioles that stay on the cortical surface and serve as conduits to more distal regions of brain also did not dilate after a penetrating arteriole occlusion (Figure 2G, two-way ANOVA on ranks, $P=0.4$). Communicating arterioles decreased slightly in both velocity and RBC flow after the clot, but did not differ significantly from penetrating arterioles (Figures 2H and 2I; two-way ANOVA on ranks, $P=0.5$ for both). Finally, we tried an alternate clotting method based on photochemical thrombosis with rose bengal, and again found no dilation in neighboring penetrating arterioles (Supplementary Text; Supplementary Figure S2). In all these experiments, urethane and isoflurane anesthetics generated similar results.

Capillaries Immediately Downstream from an Occluded Penetrating Arteriole Dilated and Slowed Dramatically

A majority of the oxygen and nutrient exchange occurs in the subsurface vessels, so we measured vessel diameter and RBC speed in parenchymal capillaries before and after occlusion of a single penetrating arteriole (Figure 3). We used only urethane for these measurements because the two anesthetics showed similar behavior in arterioles. We found a highly heterogeneous mix of diameter and speed changes in nearby capillaries after a penetrating arteriole occlusion. In the example of Figure 3, the immediate vicinity of the occluded penetrating arteriole included capillaries $\leqslant 10$ branches from the target (red in Figure 3B) and capillaries that we were unable to trace back to the target arteriole or were traced back to other arterioles (orange in Figure 3B). One capillary (marked with * in Figures 3D and 3E) was five branches away from both the target vessel and a neighboring penetrating arteriole. Note that the blood flow in this capillary was originally from the target vessel, but after the occlusion (Figure 3C), this vessel reversed direction and supplied flow from the neighboring unoccluded penetrating arteriole. Despite this source of collateral flow, there were large decreases in RBC speed in the majority of the vessels $\leqslant 10$ branches away from the occluded arteriole (Figure 3D). Interestingly, nearly all of these vessels dilated (Figure 3E).

Changes in capillary diameter and RBC speed after a penetrating arteriole clot depended strongly on the topological separation between the capillary and the occluded vessel. We categorized each measured capillary by the number of branches that separate it from the trunk of the target vessel (Figure 4A, inset), or the nearest penetrating arteriole for controls. After occlusion of a penetrating arteriole, median RBC speed slowed to 1% (4%) of the baseline speed for capillaries one to two (three to four) branches downstream from the clot (Figure 4A). The amount of slowing decreased with increased topological separation from the clotted vessel (Cuzick's trend test, $P<0.0001$), with no statistically significant slowing, relative to controls, in vessels more than four branches downstream. Capillaries one to two (three to four) branches downstream from the clot dilated to a median of 113% (110%) of baseline diameter after a penetrating arteriole clot (Figure 4B). The amount of dilation decreased further downstream from the clotted vessel (Cuzick's, $P<0.0001$), with no statistically significant dilation, relative to controls, more than four branches downstream (Figure 4B). Tube hematocrit remained unchanged after the occlusion for capillaries at all topological separations from the clotted arteriole (Supplementary Text; Supplementary Figure S3).

For capillaries with the same topological separation from the clotted vessel, the dilation and RBC speed decrease did not depend on the distance of the

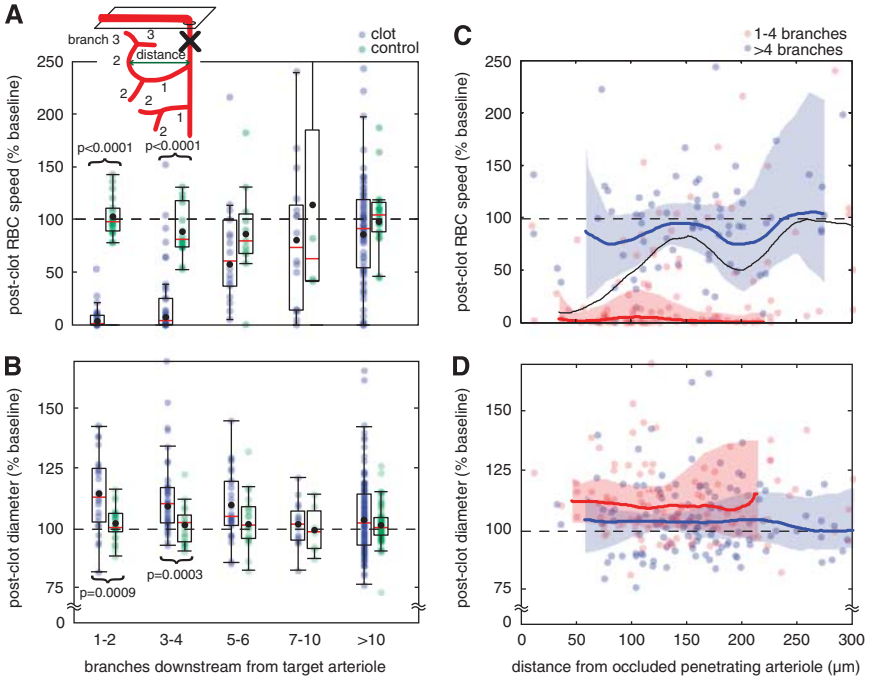

Figure 4 Dependence of capillary diameter and blood flow changes after penetrating arteriole occlusion on topological separation and spatial distance from the clotted vessel. (**A**, inset) Capillaries were categorized by the number of branches from the trunk of the occluded penetrating arteriole or, in the case of controls, from the trunk of the nearest penetrating arteriole. (**A**) Postclot red blood cell (RBC) speed, expressed as a percentage of baseline, in capillaries after penetrating arteriole occlusion or time delay only (controls). (**B**) Postclot diameter, expressed as a percentage of baseline. Points not shown in (**A**) are clot/baseline: (5 to 6 branches, 284%), (> 10, 543%); control/baseline: (3 to 4, 265%), (7 to 10, 288%), (> 10, 537%). Dependence of RBC speed (**C**) and diameter (**D**) after penetrating arteriole clot on distance from the occluded vessel. Red (blue) indicates vessels 1 to 4 (> 4) branches away from the occluded penetrating arteriole. Bold lines are running medians with 95% confidence intervals indicated by shading. Black line in (**C**) is a running median of all capillaries. Two outliers in (**C**) not shown (> 4 branches, 170 μm, 284%; > 4 branches, 73 μm, 543%). Curly brackets indicate significant differences detected with Wilcoxon–Mann–Whitney ranks sum test.

capillary from the occluded vessel. Vessels categorized as closely connected to the occluded penetrating arteriole (four or fewer branches downstream) slowed to a median speed of 2% of baseline. The speed was relatively constant for these closely connected capillaries in a 250-μm radius region around the occluded penetrating arteriole (red in Figure 4C). Distantly connected vessels (more than four branches downstream), however, remained at baseline speeds regardless of their distance from the clotted arteriole. If topological separation is ignored, the median capillary blood flow speed was severely decreased near the occluded vessel and returned to baseline over 300 μm (black line in Figure 4C), confirming previous experiments that used a different clotting method based on photochemical interactions to form occlusions (Nishimura *et al*, 2007). This gradual increase in postclot blood flow speed with distance is consistent with the decrease in the number of closely connected vessels with distance (Supplementary Text; Supplementary Figure S4). Diameter changes also showed little dependence on lateral distance from the occluded vessel, when capillaries are segregated into closely and distantly connected groups (Figure 4D). Uniformly over a 250-μm radius region around the occluded vessel, closely connected vessels dilated to a median diameter of 111% of baseline, whereas distantly connected vessels did not dilate.

We asked whether the amount of dilation after a penetrating arteriole occlusion depended on the amount of reduction in RBC speed. We plotted the postclot diameter versus postclot speed, each as a percentage of baseline, for all penetrating arterioles (Figure 5A) and capillaries (Figure 5B), including both clot and control measurements. The penetrating arteriole measurements, both clot and control, grouped into a single distribution that showed no change, on average, in either speed or diameter (Figure 5A). In the capillaries, categorization into two groups by k-means clustering (Matlab) revealed one cluster that slowed drastically and dilated (red in Figure 5B). In the second cluster (blue in Figure 5B), average speed and diameter did not change, similar to the behavior of the arterioles. This second cluster contained 91% of the control capillaries. The capillaries from clot experiments in these two clusters differed in their topological separation from the occluded penetrating arteriole (Kolmogorov–Smirnov test, $P<0.0001$), with the slowed and dilated group including more capillaries that were fewer branches from the occlusion (Figure 5B, inset).

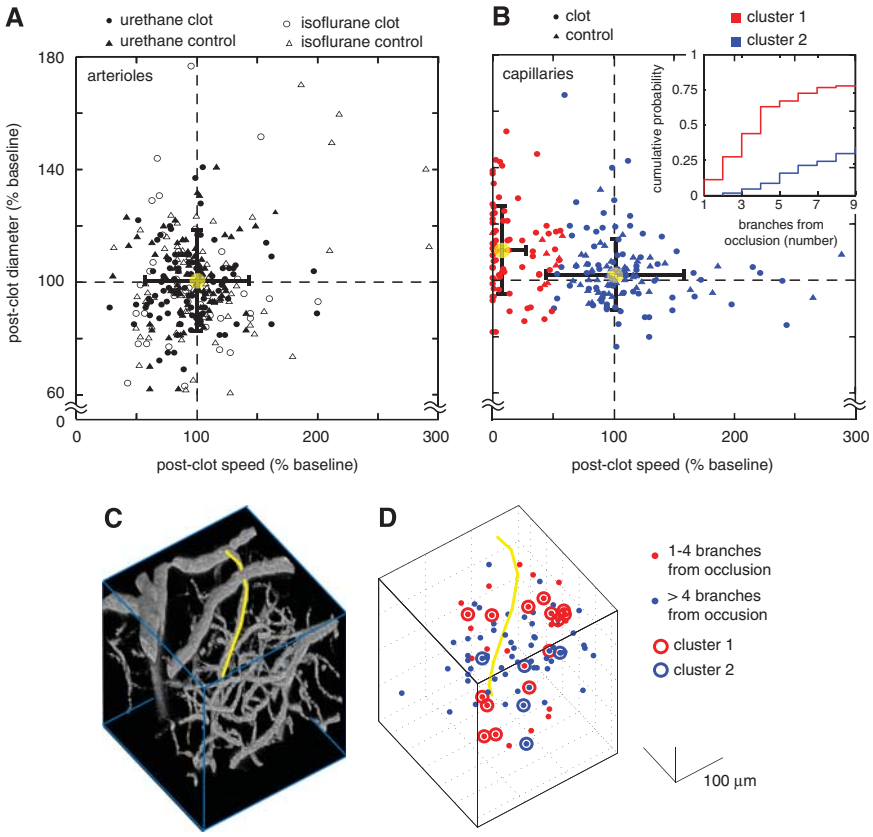

Figure 5 Large decreases in blood flow speed are linked to vasodilation. (**A**) Change in diameter versus change in centerline RBC speed in neighboring penetrating arterioles after penetrating arteriole occlusion and in control experiments. Yellow circle and lines show mean and s.d. Data points not shown in urethane clot: (51% diameter, 67% speed), urethane control: (428%, 68%), isoflurane control: (370%, 149%), (267%, 204%). (**B**) Change in diameter versus change in speed in capillaries after penetrating arteriole occlusion and in control experiments. Data were clustered by k-means into two groups (red and blue). One point not shown in control: (537%, 95%). (**B**, inset) Cumulative probability of capillaries downstream from an occluded penetrating arteriole being in the slowed and dilated (red) or unaffected (blue) cluster as a function of the topological separation between the capillary and the target vessel from 1 to 9 branches downstream. (**C**) Rendering of two-photon excited fluorescence image stack of capillaries using Voxx (Clendenon *et al*, 2002). (**D**) Capillaries from (**C**) categorized as closely (one to four branches) or distantly (more than four branches) connected to the occluded vessel with each dot centered approximately on the capillary. Circles around dots indicate categorization of the measured subset of vessels into the clusters from (**B**). In two (one) of 19 measured vessels, the topological classification suggests the vessel should slow and dilate (be unaffected) when the cluster analysis places it in the other group. Yellow line in (**C**, **D**) indicates the occluded penetrating arteriole.

For example, 88% of capillaries four or fewer branches downstream from an occluded penetrating arteriole were in the slowed and dilated cluster. The difference in the cumulative probability of being in the slowed and dilated cluster vs. the unchanged cluster was largest at four branches downstream from the occlusion (Figure 5B, inset), indicating that vessels one to four branches downstream responded, on average, differently from those more than four branches downstream.

The slowed, dilated capillaries appeared to be spatially intermingled with unaffected capillaries. The clustering analysis suggested that closely connected capillaries (four or fewer branches downstream from an occluded penetrating arteriole) tended to belong to the slowed and dilated group, whereas distantly connected capillaries (more than four branches downstream) belonged to the unchanged group (Figure 5B). Therefore, we analyzed the three-dimensional distribution of closely and distantly connected capillaries in three animals by categorizing every capillary within an image stack by its connectivity to the occluded arteriole and by the three-dimensional position of the midpoint of each capillary. In the example of Figures 5C and 5D, the flow speed and diameter changes in 19 capillaries were measured after the target penetrating arteriole was occluded, and in all but three cases, the topological classification (closely or distantly connected) correctly predicted the measured physiological response (either slowed and dilated or unchanged). This consistency supports the observed relationship between the topological classification and the vessel's response (Figure 5B, inset). In this example, many distantly connected capillaries were adjacent to closely connected vessels (Figure 5D). Across three animals, we

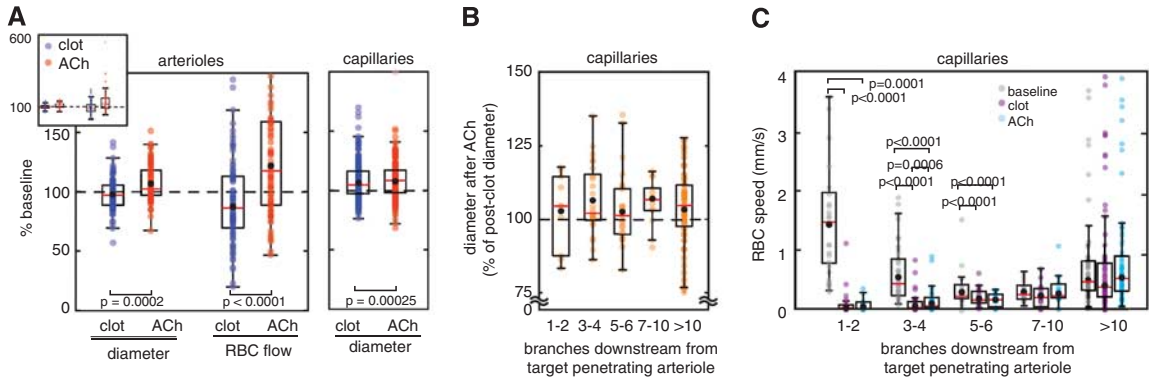

Figure 6 Changes in postclot vessel diameter and flow speed after topical application of a vasodilator (10 μmol/L acetylcholine (ACh)). (**A**) Neighboring penetrating arterioles and capillaries around an occlusion increased in diameter and in RBC flow, each expressed as a percentage of the baseline value, after topical application of ACh. Inset shows full range of data for arterioles. Arteriole clot data, shown for comparison, are same as in Figure 1, with urethane anesthesia. (**B**) Capillary diameter after ACh application, expressed as a percentage of the diameter after occlusion, as a function of the topological separation between the capillary and the occluded arteriole. Two outliers not shown at baseline: (branches 5 to 6, 65%), (> 10, 56%). (**C**) Absolute value of speeds in capillaries before, after clotting of a penetrating arteriole, and after ACh application as a function of the number of branches the capillaries are downstream from the occluded vessel. Two outliers not shown at baseline: (two branches, 5.3 mm/s), (> 10, 4.2 mm/s). Square brackets indicate significant differences with Wilcoxon ranks sum test for paired data.

find that at a distance of $\sim$120 μm from the targeted penetrating arteriole, about 16% (95% confidence interval, 10% to 24%, 1,101 vessels) of distantly connected capillaries had a capillary that was closely connected to the target penetrating arteriole as their nearest spatial neighbor (Supplementary Text; Supplementary Figure S4). The average distance between a closely connected capillary and the nearest distantly connected capillary was 46 ± 12 μm (mean $\pm$ s.d.; Supplementary Figure S5A). For the subset of distantly connected capillaries that had a closely connected vessel as a nearest neighbor, the separation between the two vessels was only 35 ± 15 μm (Supplementary Text; Supplementary Figure S5B).

Acetylcholine Application Dilated Vessels After a Penetrating Arteriole Occlusion, But Did Not Improve Flow in the Most Slowed Capillaries

After the measurements during occlusion, ACh (10 μmol/L in ACSF) was perfused into the cranial window and each vessel was remeasured in a subset of animals. Penetrating arterioles neighboring the occlusion dilated with ACh relative to the postclot diameter (Figure 6A; Wilcoxon paired rank sign test, $P = 0.0002$). The ACh also caused the RBC flow in these vessels to increase relative to the RBC flow during the occlusion (Figure 6A; Wilcoxon paired rank sign test, $P < 0.0001$). Aggregated across all measurements capillaries dilated relative to clot diameters with ACh (Figure 6A; Wilcoxon paired rank sign test, $P = 0.00025$). Capillaries with different topological separation from the occluded penetrating arteriole dilated similarly in response to ACh application (Figure 6B; Cuzick's tend test, $P = 0.85$).

With ACh application after occlusion, the median RBC speeds one to two (three to four) branches downstream from the occluded penetrating arteriole remained at <1% (13%) of baseline (Figure 6C). Ten or more branches away, the ACh causes an increase in median RBC speed to 105% of baseline values. Despite the dilation of both neighboring penetrating arterioles and capillaries, RBC speed in the downstream capillaries most affected by a penetrating arteriole occlusion was not substantially improved by ACh, whereas distantly connected vessels became slightly hyperemic. Similarly, RBC flux, the number of RBCs flowing through the capillary segment per unit time, decreased severely in the capillaries closest to the occlusion, and was not improved with ACh application (Supplementary Text; Supplementary Figure S6).

Discussion

Targeted Femtosecond Laser Ablation Provides a Viable Technique for Forming Clots in Individual Penetrating Arterioles

Femtosecond laser ablation can trigger clotting in penetrating arterioles while preserving structure and flow in neighboring vessels, enabling the study of physiological processes, such as vasoreactivity, in the nearby microvessels. This laser ablation technique is a variation on the method previously developed to clot single cortical capillaries (Nishimura *et al*, 2006). As the interaction of the laser light and the tissue depends on nonlinear absorption, only the targeted portion of the vessel is injured by the laser and the subsequent clotting and occlusion are limited to a single vascular segment. Previous work

on occlusions of penetrating arterioles used photochemical thrombosis with rose bengal (Nishimura *et al*, 2007). As the rose bengal method uses linear optical excitation to produce the singlet oxygen that damages the vessel wall and initiates clotting, it is not possible to confine the effect to a single vessel segment and some level of clotting in surrounding capillaries is very difficult to avoid. To rule out the possible effects of our clotting technique on vasoreactivity, we tested both the femtosecond laser ablation and photochemical methods for clotting penetrating arterioles and saw no dilation in neighboring penetrating arterioles for both methods (Supplementary Figure S2). In addition, previous measurements of flow changes in capillaries after a penetrating arteriole occlusion produced using the rose bengal method (Nishimura *et al*, 2007) are similar to those reported here (Figures 4A and 4C).

Neighboring Penetrating Arterioles Do Not Dilate to Compensate for Penetrating Arteriole Occlusion

We used 2PEF microscopy to investigate whether active vascular regulation in surrounding penetrating arterioles mitigates the decreased flow in capillaries downstream from an occluded cortical penetrating arteriole. We first investigated whether the neighboring penetrating arterioles that feed territories adjacent to the occluded vessel dilate in response to the occlusion (Figure 1). Contrary to the expectation that the occlusion could trigger a compensatory vasoactive response in the surrounding area, the neighboring penetrating arterioles did not dilate (Figure 1F). Even the closest arterioles, both in topological and spatial distance, did not dilate after occlusion (Figure 2). Our methods had sufficient statistical power (Supplementary Text) to resolve changes in arteriole diameter and RBC speed of a magnitude comparable to or smaller than those observed in neurovascular coupling. Taken together, this data suggest that it is unlikely there is any physiologically relevant compensatory vasoregulatory mechanism that is recruited to increase flow in neighboring penetrating arterioles to increase perfusion in the tissue adjacent to the occluded arteriole.

This absence of dilation is in marked contrast to the coordinated dilation of local and upstream arterioles that occurs in response to increases in neural activity (Devor *et al*, 2008; Iadecola *et al*, 1997). Upstream dilation of arterioles in neurovascular coupling (and other systems such as muscle) is likely to be mediated by signal conduction in the endothelium (Dietrich *et al*, 1996; Welsh and Segal, 1998) or astrocytes (Xu *et al*, 2008). Our observation of dilation in the neighboring penetrating arterioles after ACh application (Figure 6A), an endothelium-dependent dilator (Faraci and Heistad, 1998; Rosenblum and Nelson, 1988), indicates that both endothelium and smooth muscle were functional despite experimental manipulations. This suggests that the lack of dilation after penetrating arteriole occlusion comes from a lack of signaling. Although we used two different mechanisms for clotting that show similar results, we cannot eliminate the possibility that the lack of dilation of neighboring arterioles after the clot is an artifact of our technique. Injured endothelial cells or astrocytes at the clot location might not be capable of conducting the vasodilatory signals that might otherwise be present (Emerson and Segal, 2000; Xu *et al*, 2008). However, because these cells are quite susceptible to ischemia or hypoxia (Fisher, 2008), it is likely that a naturally forming thrombus or an embolus would also result in a disruption of endothelial or astrocyte function that would interfere with any possible vasodilatory signal (Emerson and Segal, 2000).

Vessel Dilation Is Correlated with Large Flow Speed Decreases

Although no dilation was observed in arterioles, a subset of capillaries do dilate after the occlusion (Figures 4B and 4D). Cluster analysis of downstream capillaries suggests that there is a trend for lower flow to be associated with a larger dilation (Figure 5B). No such trend is observed in the neighboring penetrating arterioles (Figure 5A), but this may be explained by the fact that after a single penetrating arteriole occlusion, flow in other arterioles does not drop to the extremely low levels observed in the downstream capillaries. After larger strokes, such as MCA occlusions, other investigators do observe acute vasodilation in the surface and penetrating arterioles that sit downstream from the occlusion (Belayev *et al*, 2002; Shih *et al*, 2009; Tomita *et al*, 2005; Wei *et al*, 1998), consistent with the idea that drastically reduced flow or intraluminal pressure is necessary to trigger dilation. In the work by Shih *et al* (2009), mean velocities in penetrating arterioles dropped to $\sim$30% of baseline and vessel diameter increased to $\sim$120% of baseline after MCA occlusion. Wei *et al* (1998) made ministrokes by ligating several surface arterioles and noted a marked dilation and also described considerable slowing in nearby surface arterioles. Taken together, these data suggest that the vasodilation signal does not activate in a vessel until hemodynamics have substantially changed in that vessel.

Spatial Heterogeneity in Capillary Dilation Suggests that the Vasodilatory Signal Is Not of Parenchymal Origin

The spatial distribution of dilated and undilated capillaries rules out a parenchymal source for the vasodilation signal. There are frequent occurrences in which an extremely slowed and dilated capillary is adjacent to a rapidly flowing and undilated capillary. This is reflected in the aggregate data as a strong dependence of the speed and diameter

changes on the topological separation (Figures 4A and 4B), but not the spatial distance (Figures 4C and 4D) between a capillary and the occluded penetrating arteriole. Analysis of the spatial distribution of vessels with different topological separation (Supplementary Figures S4 and S5) shows that capillaries only a few branches downstream from the target, which slow and dilate after the occlusion, are spatially interspersed with more distantly connected capillaries, which are largely unaffected by the clot (Figures 5C and 5D). The close proximity of dilated and unaffected capillaries suggests that there is no signal for vasodilation that originates from the neurons or astrocytes or other parenchymal cells. If such a diffusible signal from the parenchymal tissue existed, one would expect that capillaries spatially near but many branches away from the occluded arteriole would dilate along with nearby, but more closely connected vessels.

Past work using a pimonadozole probe that precipitates in severe hypoxia suggests that tissue within 150 μm of a penetrating arteriole occlusion is relatively uniformly hypoxic (Nishimura *et al*, 2007). Our observations of undilated vessels in this region suggest vessels that maintain high levels of flow do not dilate even if they run through regions of likely hypoxia near the occluded vessel. This argues that tissue hypoxia is not sufficient to drive vasodilation. Current ideas that neurovascular coupling in the normal brain is linked to synaptic release and byproducts of neuronal activity rather than to metabolism or oxygen usage are consistent with our findings (Attwell and Iadecola, 2002; Devor *et al*, 2008; Lindauer *et al*, 2009; Sukhotinsky *et al*, 2010). For example, recent work on neurovascular coupling shows blood flow still increases in regions of neuronal activity even under hyperbaric hyperoxygenation, which demonstrates another case in which dexoygenation is decoupled from vasodilation (Lindauer *et al*, 2009). We find that the alterations in oxygenation and energy delivery caused by blood flow decreases due to a penetrating arteriole occlusion do not generate upstream or diffusible vasodilatory signals, even though the oxygenation and metabolite deficits due to occlusions are more severe than those caused by normal neuronal activity.

Dilation in Capillaries Downstream from a Penetrating Arteriole Occlusion Is Triggered by a Vasogenic Signal, Likely Changes in Transmural Pressure

The dilation in downstream capillaries after penetrating arteriole occlusion (Figure 4B) suggests that there is a perfusion-dependent signal for dilation. Possible candidates for the vasodilatory signal include flow-dependent forces such as changes in shear stress or transmural pressure. Arterioles do respond to changes in shear stress, but arterioles tend to dilate in response to an increase in shear stress (Ngai and Winn, 1995). This response is the opposite of what is observed in the capillaries in our experiments and in surface and penetrating arterioles after MCA occlusion (Belayev *et al*, 2002; Shih *et al*, 2009; Tomita *et al*, 2005; Wei *et al*, 1998) in which vessels dilate in response to decreased flow. Hematocrit in the capillaries did not change significantly after occlusion (Supplementary Text; Supplementary Figure S3), but the RBC flux did drop in proportion to the speed change, suggesting that dilated capillaries may respond to some change in the rate of RBCs that pass through (Supplementary Text; Supplementary Figure S6). A more likely candidate is change in transmural pressure. Brain arterioles constrict with increased pressure, suggesting that decreased transmural pressure could trigger dilation (Ngai and Winn, 1995; Schmid-Schonbein, 1999). The vessels immediately downstream from a penetrating arteriole are likely at reduced luminal pressure after the occlusion relative to before the occlusion because these vessels are now effectively farther downstream from a high-pressure arteriole. Similarly, surface and penetrating arterioles would be at reduced luminal pressure after MCA occlusion, suggesting that a myogenic mechanism for vasodilation could be also responsible for the acute dilation observed after large stroke models (Belayev *et al*, 2002; Shih *et al*, 2009; Tomita *et al*, 2005; Wei *et al*, 1998). Thus, our work suggests that acute postclot vascular reactivity could use the same mechanisms involved in autoregulation, which keeps brain perfusion constant under changing systemic blood pressure.

Hemodynamic Arguments Against Vasodilators as Therapies for Microvascular Strokes

We applied a vasodilator, ACh, to investigate whether increasing flow in unoccluded arterioles can substantially improve flow in capillaries downstream from an occluded penetrating arteriole (Figure 6). Despite dilation in both neighboring penetrating arterioles and capillaries, ACh did not substantially improve perfusion in the territory of decreased flow caused by the occlusion. The ACh leads to only a very small increase in the magnitude of RBC speed (Figure 6C). The first few branches downstream from the occlusion are most severely affected by the clot and are also the least improved by vasodilator application. This result suggests that although connections between penetrating arteriole territories through the capillary bed exist (Moody *et al*, 1990), they are too infrequent to provide flow between territories. Clinical trials for vasodilators such as xanthine derivatives for treatment of vascular dementia (Kittner *et al*, 1997; Pantoni, 2004) have not shown significant efficacy and have also been disappointing for the treatment of stroke (Bath and Bath-Hextall, 2004; Bereczki and Fekete, 2008). If vascular dementia is driven by the effects of many small vessel occlusions, our finding that ACh does

not improve flow downstream from the occlusion might be a contributing factor to the drug trials' somewhat disappointing results. However, we cannot rule out that other patterns of dilation driven by mechanisms other than ACh might be more effectual or that vasodilators might have significant impact in the case of partial occlusions. Alternative strategies for increasing flow include reducing blood viscosity (Nishimura *et al*, 2006) or leukocyte adhesion (Belayev *et al*, 2002), each of which have been found to increase flow downstream from local occlusions. However, it is not clear that these flow increases are sufficient to be therapeutic.

Disclosure/conflict of interest

The authors declare no conflict of interest.

References

Attwell D, Iadecola C (2002) The neural basis of functional brain imaging signals. *Trends Neurosci* 25:621–5

Bath PM, Bath-Hextall FJ (2004) Pentoxifylline, propentofylline and pentifylline for acute ischaemic stroke. *Cochrane Database Syst Rev*; CD000162

Belayev L, Pinard E, Nallet H, Seylaz J, Liu Y, Riyamongkol P, Zhao W, Busto R, Ginsberg MD (2002) Albumin therapy of transient focal cerebral ischemia: *in vivo* analysis of dynamic microvascular responses. *Stroke* 33:1077–84

Bereczki D, Fekete I (2008) Vinpocetine for acute ischaemic stroke. *Cochrane Database Syst Rev*; CD000480

Blinder P, Shih AY, Rafie C, Kleinfeld D (2010) Topological basis for the robust distribution of blood to rodent neocortex. *Proc Natl Acad Sci USA* 107:12670–5

Clendenon JL, Phillips CL, Sandoval RM, Fang S, Dunn KW (2002) Voxx: a PC-based, near real-time volume rendering system for biological microscopy. *Am J Physiol Cell Physiol* 282:C213–8

Coyle P, Heistad DD (1987) Blood flow through cerebral collateral vessels one month after middle cerebral artery occlusion. *Stroke* 18:407–11

Cuzick J (1985) A Wilcoxon-type test for trend. *Stat Med* 4:87–90

Devor A, Hillman EM, Tian P, Waeber C, Teng IC, Ruvinskaya L, Shalinsky MH, Zhu H, Haslinger RH, Narayanan SN, Ulbert I, Dunn AK, Lo EH, Rosen BR, Dale AM, Kleinfeld D, Boas DA (2008) Stimulus-induced changes in blood flow and 2-deoxyglucose uptake dissociate in ipsilateral somatosensory cortex. *J Neurosci* 28:14347–57

Dietrich HH, Kajita Y, Dacey RG Jr (1996) Local and conducted vasomotor responses in isolated rat cerebral arterioles. *Am J Physiol* 271:H1109–16

Emerson GG, Segal SS (2000) Endothelial cell pathway for conduction of hyperpolarization and vasodilation along hamster feed artery. *Circ Res* 86:94–100

Faraci FM, Heistad DD (1998) Regulation of the cerebral circulation: role of endothelium and potassium channels. *Physiol Rev* 78:53–97

Faul F, Erdfelder E, Lang AG, Buchner A (2007) G*Power 3: a flexible statistical power analysis program for the social, behavioral, and biomedical sciences. *Behav Res Methods* 39:175–91

Fisher M (2008) Injuries to the vascular endothelium: vascular wall and endothelial dysfunction. *Rev Neurol Dis* 5(Suppl 1):S4–11

Iadecola C, Yang G, Ebner TJ, Chen G (1997) Local and propagated vascular responses evoked by focal synaptic activity in cerebellar cortex. *J Neurophysiol* 78:651–9

Kittner B, Rossner M, Rother M (1997) Clinical trials in dementia with propentofylline. *Ann NY Acad Sci* 826:307–16

Kleinfeld D, Delaney KR (1996) Distributed representation of vibrissa movement in the upper layers of somatosensory cortex revealed with voltage sensitive dyes. *J Comp Neurol* 375:89–108

Kleinfeld D, Mitra PP, Helmchen F, Denk W (1998) Fluctuations and stimulus-induced changes in blood flow observed in individual capillaries in layers 2 through 4 of rat neocortex. *Proc Natl Acad Sci USA* 95:15741–6

Kovari E, Gold G, Herrmann FR, Canuto A, Hof PR, Michel JP, Bouras C, Giannakopoulos P (2004) Cortical microinfarcts and demyelination significantly affect cognition in brain aging. *Stroke* 35:410–4

Lindauer U, Leithner C, Kaasch H, Rohrer B, Foddis M, Fuchtemeier M, Offenhauser N, Steinbrink J, Royl G, Kohl-Bareis M, Dirnagl U (2009) Neurovascular coupling in rat brain operates independent of hemoglobin deoxygenation. *J Cereb Blood Flow Metab* 30:757–68

Moody DM, Bell MA, Challa VR (1990) Features of the cerebral vascular pattern that predict vulnerability to perfusion or oxygenation deficiency: an anatomic study. *AJNR Am J Neuroradiol* 11:431–9

Muller M, Squier J, Wolleschensky R, Simon U, Brakenhoff GJ (1998) Dispersion pre-compensation of 15 femtosecond optical pulses for high-numerical-aperture objectives. *J Microsc* 191:1141–50

Ngai AC, Winn HR (1995) Modulation of cerebral arteriolar diameter by intraluminal flow and pressure. *Circ Res* 77:832–40

Nguyen QT, Tsai PS, Kleinfeld D (2006) MPScope: a versatile software suite for multiphoton microscopy. *J Neurosci Methods* 156:351–9

Nishimura N, Schaffer CB, Friedman B, Lyden PD, Kleinfeld D (2007) Penetrating arterioles are a bottleneck in the perfusion of neocortex. *Proc Natl Acad Sci USA* 104:365–70

Nishimura N, Schaffer CB, Friedman B, Tsai PS, Lyden PD, Kleinfeld D (2006) Targeted insult to subsurface cortical blood vessels using ultrashort laser pulses: three models of stroke. *Nat Methods* 3:99–108

Ogawa S, Lee T-m, Nayak AS, Glynn P (1990) Oxygenation-sensitive contrast in magnetic resonance image of rodent brain at high fields. *Magn Reson Med* 14:68–78

Pantoni L (2004) Treatment of vascular dementia: evidence from trials with non-cholinergic drugs. *J Neurol Sci* 226:67–70

Park L, Zhou P, Pitstick R, Capone C, Anrather J, Norris EH, Younkin L, Younkin S, Carlson G, McEwen BS, Iadecola C (2008) Nox2-derived radicals contribute to neurovascular and behavioral dysfunction in mice overexpressing the amyloid precursor protein. *Proc Natl Acad Sci USA* 105: 1347–52

Rosenblum WI, Nelson GH (1988) Endothelium-dependent constriction demonstrated *in vivo* in mouse cerebral arterioles. *Circ Res* 63:837–43

Schaffer CB, Friedman B, Nishimura N, Schroeder LF, Tsai PS, Ebner FF, Lyden PD, Kleinfeld D (2006) Two-photon

imaging of cortical surface microvessels reveals a robust redistribution in blood flow after vascular occlusion. *PLoS Biol* 4:e22

Schmid-Schonbein GW (1999) Biomechanics of microcirculatory blood perfusion. *Annu Rev Biomed Eng* 1:73–102

Shih AY, Friedman B, Drew PJ, Tsai PS, Lyden PD, Kleinfeld D (2009) Active dilation of penetrating arterioles restores red blood cell flux to penumbral neocortex after focal stroke. *J Cereb Blood Flow Metab* 29:738–51

Sigler A, Goroshkov A, Murphy TH (2008) Hardware and methodology for targeting single brain arterioles for photothrombotic stroke on an upright microscope. *J Neurosci Methods* 170:35–44

Sukhotinsky I, Yaseen MA, Sakadzic S, Ruvinskaya S, Sims JR, Boas DA, Moskowitz MA, Ayata C (2010) Perfusion pressure-dependent recovery of cortical spreading depression is independent of tissue oxygenation over a wide physiologic range. *J Cereb Blood Flow Metab* 30:1168–77

Tomita Y, Kubis N, Calando Y, Tran Dinh A, Meric P, Seylaz J, Pinard E (2005) Long-term *in vivo* investigation of mouse cerebral microcirculation by fluorescence confocal microscopy in the area of focal ischemia. *J Cereb Blood Flow Metab* 25:858–67

Vander Eecken HM, Adams RD (1953) The anatomy and functional significance of the meningeal arterial anastomoses of the human brain. *J Neuropathol Exp Neurol* 12:132–57

Vermeer SE, Prins ND, den Heijer T, Hofman A, Koudstaal PJ, Breteler MM (2003) Silent brain infarcts and the risk of dementia and cognitive decline. *N Engl J Med* 348:1215–22

Watson BD, Dietrich WD, Busto R, Wachtel MS, Ginsberg MD (1985) Induction of reproducible brain infarction by photochemically initiated thrombosis. *Ann Neurol* 17:497–504

Wei L, Craven K, Erinjeri J, Liang GE, Bereczki D, Rovainen CM, Woolsey TA, Fenstermacher JD (1998) Local cerebral blood flow during the first hour following acute ligation of multiple arterioles in rat whisker barrel cortex. *Neurobiol Dis* 5:142–50

Welsh DG, Segal SS (1998) Endothelial and smooth muscle cell conduction in arterioles controlling blood flow. *Am J Physiol* 274:H178–86

Xu HL, Mao L, Ye S, Paisansathan C, Vetri F, Pelligrino DA (2008) Astrocytes are a key conduit for upstream signaling of vasodilation during cerebral cortical neuronal activation *in vivo*. *Am J Physiol Heart Circ Physiol* 294:H622–32

Supplementary Information accompanies the paper on the Journal of Cerebral Blood Flow & Metabolism website (http://www.nature.com/jcbfm)